Gated Conditional Displacement Readout of Superconducting Qubits

S. Touzard, A. Kou, N. E. Frattini, V. V. Sivak, S. Puri, A. Grimm, L. Frunzio, S. Shankar, and M. H. Devoret

Phys. Rev. Lett. **122**, 080502 — Published 25 February 2019

DOI: 10.1103/PhysRevLett.122.080502

Gated conditional displacement readout of superconducting qubits

S. Touzard,[1,*] A. Kou,[1] N.E. Frattini,[1] V.V. Sivak,[1] S. Puri,[2]
A. Grimm,[1] L. Frunzio,[1] S. Shankar,[1] and M.H. Devoret[1,†]

[1] *Department of Applied Physics and Physics, Yale University, New Haven, CT 06520, USA*
[2] *Yale Quantum Institute, Yale University, New Haven, CT 06520, USA*

(Dated: January 28, 2019)

We have realized a new interaction between superconducting qubits and a readout cavity that results in the displacement of a coherent state in the cavity, conditioned on the state of the qubit. This conditional state, when it reaches the cavity-following, phase-sensitive amplifier, matches its measured observable, namely the in-phase quadrature. In a setup where several qubits are coupled to the same readout resonator, we show it is possible to measure the state of a target qubit with minimal dephasing of the other qubits. Our results suggest novel directions for faster readout of superconducting qubits and implementations of bosonic quantum error-correcting codes.

Measuring the state of a qubit is a fundamental operation of quantum physics and a primitive for building a universal quantum computer [1]. Over the years, non-destructive strategies to measure one given system at the scale of a single quantum of energy have been devised and tested, first with Rydberg atoms [2]. In circuit quantum electrodynamics (cQED), such quantum non-demolition (QND) readout schemes are currently based on a dispersive interaction: the phase of a coherent state of a microwave pulse is shifted depending on the state of the qubit [3–5]. In the best cases, this phase is then indirectly measured using a phase-sensitive amplifier to record the quadrature along which the two phase-shifted coherent states are separated. In order to achieve faster high-fidelity measurement, this separation can be augmented by increasing the number of probing photons. Unfortunately, in practice, driving with more photons induces unwanted qubit transitions and does not improve significantly the overall fidelity of the readout process [6–9].

To circumvent the flaws of the RF dispersive qubit readout, a new paradigm has been proposed [10–12], which consists of two ideas. First, the Z component (energy operator) of the qubit needs to be directly coupled to the quadrature measured by a phase-sensitive amplifier, which does not in principle degrade the signal-to-noise ratio (SNR). This bare interaction has been referred to as "longitudinal" [10, 11]. Such interaction is, in fact, similar to that associated with radiation pressure in optomechanics [13]. Second, the interaction needs to be modulated in time, at the frequency of the readout cavity mode [12]. This modulation of the coupling creates a displacement of the cavity that is conditioned on the state of the qubit. Input squeezed light can further enhance the sensitivity [12, 14]. Alternatively, the coupling can be modulated in a stroboscopic way to avoid the back-action of the microwave field [14–17]. The bare longitudinal interaction has been realized experimentally with superconducting circuits [18–20] but, in absence of the frequency modulation, it has not yet led to a QND microwave readout.

In this letter, we report the realization of such a conditional displacement readout using detuned parametric pumping of the Josephson Hamiltonian of a transmon [21]. This latter technique is a practical alternative to the flux modulation that has been proposed theoretically [10–12]. As shown in [22], the time-dependent qubit-cavity Hamiltonian, in the doubly rotating frame, is given by

$$\frac{\mathbf{H}_{\text{eff}}}{\hbar} = -\frac{\alpha}{2}\mathbf{q}^{\dagger 2}\mathbf{q}^2 + \zeta(t)(\mathbf{q}^\dagger\mathbf{q} - \mathbf{1}/2)(\mathbf{c}+\mathbf{c}^\dagger) - \chi(\mathbf{q}^\dagger\mathbf{q})(\mathbf{c}^\dagger\mathbf{c}), \tag{1}$$

where α is the anharmonicity of the transmon qubit ($\mathbf{q}$) and χ is its dispersive coupling to the readout cavity ($\mathbf{c}$). The second term is the same as a resonant longitudinal interaction of strength ζ between the transmon qubit and the readout cavity. With this implementation, the interaction is gated: it can be instantly switched on/off, and is qubit-selective. We exploit this latter feature to read the state of a single target qubit when multiple other qubits are coupled to the same resonator. We show that the target qubit can be measured non-destructively 98.4% of the time, with minimal detrimental effects on the other qubits of the system. In principle, the same scheme can measure several qubits at the same time by engineering a similar interaction on several target qubits but with a different phase [12].

The principle of the experiment is shown in Fig. 1(a). A superconducting qubit is weakly coupled to a low-Q microwave resonator such that their residual dispersive interaction χ is much smaller than the linewidth κ [3]. This so-called weak dispersive regime [23] is desirable since it mitigates the Purcell effect [24], the dephasing due to spurious thermal photons [25, 26], and, more generally, any spurious coupling to other qubits through the cavity mode. However, the weak dispersive regime is usually unfavorable for qubit readout because it results in a slow measurement rate and, furthermore, requires populating the resonator with a large number of photons. This is a disadvantage in multi-qubit systems where photons in the shared resonator lead to unwanted decoherence in

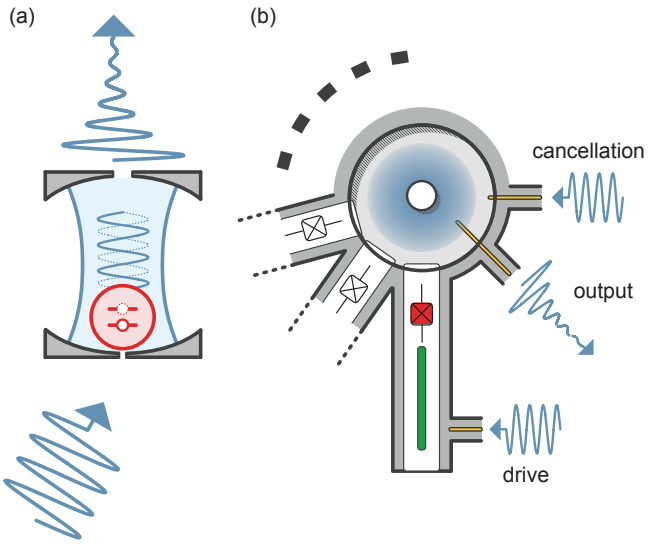

FIG. 1. (a) Principle of the experiment. A schematic superconducting two-level artificial atom (red) is placed where the field of a cavity (blue) is weak, for instance close to a partially transmitting mirror, to be in the weak coupling regime. When the atom is driven at the frequency of the cavity, the electromagnetic field of the cavity is spontaneously displaced with a sense which depends on the state of the atom (dotted or solid line) and exits through the main aperture. (b) Multi-qubit architecture. An arbitrary number of transmon chips are placed around the field of an aluminum post-cavity (three chips in the current experiment). The target transmon (red) is driven through a filter mode (green) which is coupled to a microwave input coupler. The number of photons in the cavity is kept minimal using a cancellation port (see text). The field of the cavity is measured using the strongly-coupled output port.

the qubits that are not being addressed. Here, we realize a fast readout while avoiding these drawbacks by implementing the aforementioned novel idea of conditional displacement readout. In our system a transmon is driven at the frequency of the cavity (Fig. 1(a)), resulting in the effective resonant longitudinal interaction. For a drive with an envelope of amplitude $\bar{\epsilon}(t)$ and a detuning Δ between the two modes, an analysis of the full Josephson Hamiltonian [22] gives

$$\zeta(t) = \sqrt{2\alpha\chi}\frac{\bar{\epsilon}(t)}{\Delta}.$$

Since the strength ζ of this interaction depends on the product $\alpha\chi$, rather than χ, it is possible to increase ζ while maintaining χ small. Thus, a readout that is much faster than the qubit relaxation time is obtained while keeping the advantages of the weak dispersive coupling.

We demonstrate these features using an aluminum cylindrical post-cavity [27] as a readout cavity ($\omega_c/2\pi = 8.0\,\mathrm{GHz}$) coupled to three transmon qubits (Fig. 1(b)). Our scheme is also compatible with a 2D architecture and a larger number of qubits. The target qubit ($\omega_q/2\pi = 4.9\,\mathrm{GHz}$) is coupled on one side to a stripline resonator ($\omega_f/2\pi = 6.4\,\mathrm{GHz}$), which is used as a filter mode with two roles. First, the filter mode is well-coupled both to the drive input pin (with coupling $\kappa_c/2\pi \approx 8\,\mathrm{kHz}$) and to the qubit ($\chi_{qf}/2\pi = 2.5\,\mathrm{MHz}$) so that we can drive the qubit strongly off-resonance without limiting its coherence through the Purcell effect. Second, the presence of the filter mode increases the physical distance between the drive pin and the readout cavity and limits their direct coupling to much less than 1 kHz. To minimize the number of photons in the readout cavity introduced by this finite direct coupling, a phase-locked cancellation drive is applied to a cancellation port (with coupling $\kappa_c/2\pi \approx 5\,\mathrm{kHz}$). Finally, the field is picked up by a strongly coupled output port which connects the cavity to a phase-sensitive amplifying chain [28] and to room temperature electronics [22]. We adjust the output coupling pin of the readout cavity in order to get an emission rate $\kappa = (100\,\mathrm{ns})^{-1}$, which sets the characteristic time of our measurement. The target qubit is characterized by an anharmonicity $\alpha/2\pi = 221\,\mathrm{MHz}$ and is coupled to the cavity with a residual $\chi/2\pi \approx 100\,\mathrm{kHz}$ ($\chi \approx \kappa/16$). Two other qubits with similar parameters are coupled to the same cavity. We observe a range of qubit energy relaxation times T_1 between 90 µs - 190 µs, which vary, not atypically, from sample to sample. We present the data acquired for a qubit with $T_1 = 90\,\mu\mathrm{s}$. The T_2-echo of our transmon varies between cooldowns in the range of 30 µs to 170 µs, for reasons which have not yet been pinned down, but which we believe to be independent from the effect we are demonstrating.

In order to quantify the strength of the resonant longitudinal interaction, we turn on the drive for 2 µs and acquire 3×10^5 trajectories with the target qubit initialized in $|g\rangle$ and $|e\rangle$. The signal is amplified at low temperature using a phase-sensitive amplifier. We use the ensemble average response for these two cases to determine the optimal demodulation envelope $(\bar{I}_{|e\rangle} - \bar{I}_{|g\rangle} - i(\bar{Q}_{|e\rangle} - \bar{Q}_{|g\rangle}))$ [29, 30], where the bar indicates the ensemble average. The optimal envelope is used to weigh single-shot trajectories and extract the SNR as a function of demodulation time. The SNR in amplitude, plotted in Fig. 2(b), is fit to the theoretical SNR for a conditional displacement demodulated with the optimal envelope [22]. The theory is only adjusted by an overall factor, which depends both on the efficiency $\eta = 0.6$ of the amplification chain, extracted independently [22, 31], and the number $|\alpha_m|^2$ of measuring photons in steady-state (Fig. 2(a)). We estimate from the fit of the SNR $|\alpha_m|^2 = 2.6$ photons, which corresponds to a coupling strength $\zeta_0/2\pi = \alpha_m\kappa/8\pi = 1.28\,\mathrm{MHz}$ for the pulse of constant amplitude.

In the same plot, we compare the SNR of the displacement readout to the theoretical SNR of ideal dispersive readout with $\chi = \kappa$, using identical efficiency η and pho-

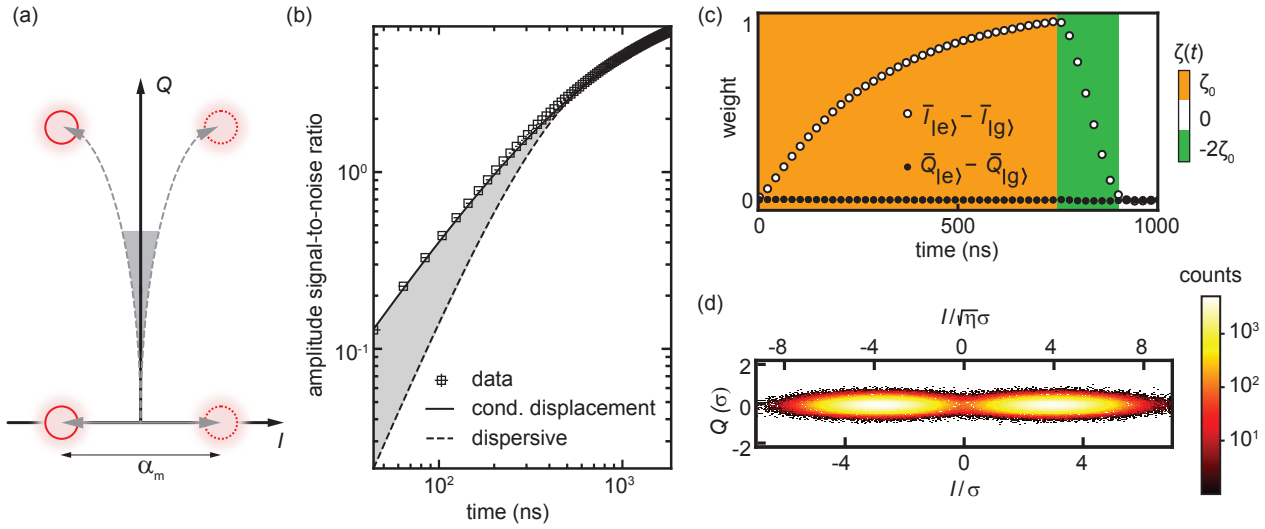

FIG. 2. Conditional coherent states separation. (a) Phase-space representation of this separation under an RF pulse implementing our engineered interaction (gray solid line) and under an RF pulse driving the cavity directly (gray dashed line). In the former case, the field of the cavity is displaced along the I quadrature with a sense that depends on the state of the transmon. The distance between the two possible steady states is noted α_m. In the latter case, the cavity state would be displaced unconditionally along Q and conditionally along I. The gray area indicates that at small times, the two coherent states do not separate. (b) Log-Log plot of the amplitude SNR as a function of time. The data are fitted with the theoretical SNR for a conditional displacement (solid line), adjusted in amplitude with the efficiency η, determined independently, and with a fit parameter corresponding to the coupling strength. The dashed line corresponds to the optimal dispersive readout with the same parameters and $\chi = \kappa$. The gray area corresponds to the delay shown in (a). (c) Demodulation envelope comprising a depletion section. The coupling strength varies from ζ_0 for 750 ns (orange), to $-2\zeta_0$ for 120 ns (green). (d) Histogram of the demodulated signal. The axis are calibrated using the calibrated efficiency η and the width σ of the Gaussians along the x-axis. The squeezing is due to the amplifier being phase-sensitive.

ton number $|\alpha_m|^2$. In steady-state, by construction, the performance of both readouts converge to the same value $\propto (\kappa\tau)^{1/2}$. However, for the dispersive readout, the SNR grows much slower for initial times ($\kappa\tau \ll 1$). This can be understood from the initial cavity response, as shown in Fig. 2(a). For the dispersive readout, the cavity coherent state first rings up along the Q quadrature at rate κ and then separates, along the I quadrature, at rate χ, into the $|g\rangle$ and $|e\rangle$ components. On the other hand, for the conditional displacement readout, the two coherent states are displaced directly at rate κ. As the measurement is sensitive only to the separation, the conditional displacement readout is faster for short times.

The direct separation of the two coherent states along a single quadrature, as depicted in Fig. 2(a), is obtained for the optimal envelope, shown in Fig. 2(c) for a specific readout pulse length of 750 ns. By construction, the signal is contained within the I quadrature and no response develops along Q. Furthermore, to speed-up the measurement, we evacuate, near the end of the readout sequence, the cavity by reversing the amplitude of the pulse and hence, the strength of the coupling to $-2\zeta_0$ for 120 ns. A similar trick had been previously demonstrated for the dispersive case [31, 32].

To quantify the discrimination power of the readout, we show in Fig. 2(d) the histogram corresponding to 1.5×10^6 single-shot measurements demodulated with the optimal envelope. The bottom x-axis is normalized by the apparent standard deviation of the two distributions, whereas the top x-axis is re-normalized with a factor $\sqrt{\eta}$ to depict the losses in the measurement chain. Since our setup uses a phase-sensitive amplifier to amplify along the I quadrature, the distribution is squeezed along the Q quadrature, which does not contain any information. The distributions along I are separated by 5.8 standard deviations, corresponding to a discrimination power of 99.5%.

Although a good discrimination power is necessary, it is not sufficient to assess the overall merit of the readout. We further characterize the readout using two metrics: (1) the fidelity $\mathcal{F}$, which quantifies how accurately the measurement assigns the state prepared before the readout, and (2) the quantum-non-demolition metric $\mathcal{Q}$ (QND-ness), which quantifies how likely a qubit is to adopt its measured state after the readout. These metrics will be smaller than the discrimination power due to the qubit transitions during the readout, due themselves to either T_1 or induced by the drive. To estimate the two metrics, we perform a train of measurement pulses with no delay (Fig. 3(a)). The vast majority of mea-

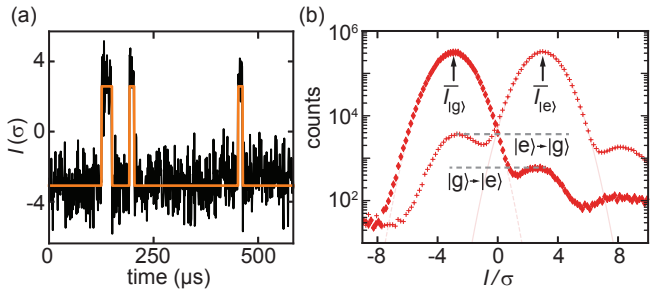

FIG. 3. Quantum-non-demolition readout. (a) Results of successive single-shot measurements displaying 6 discrete jumps (black). The orange trace is a guide for the eye and is obtained with a latching filter applied to the data. The correlation between successive measurements indicates that the readout is non-destructive. (b) Histogram of the demodulated signal along the I quadrature with post-selecting the qubit in $|g\rangle$ (diamonds) and in $|e\rangle$ (crosses). The two distributions are fitted with Gaussians (light red, dashed and solid lines). When the qubit starts in $|g\rangle$ (resp. $|e\rangle$) it mostly persists in $|g\rangle$ (resp. $|e\rangle$). The gray dashed lines emphasize the number of jumps from $|g\rangle$ (resp. $|e\rangle$) to $|e\rangle$ (resp. $|g\rangle$).

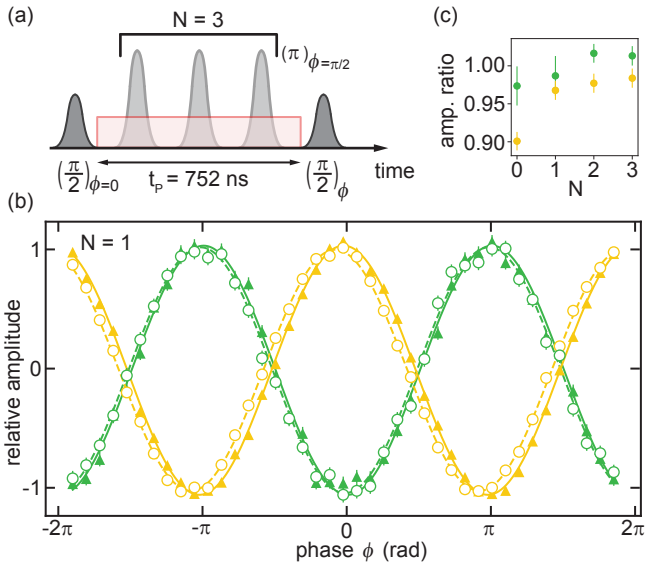

FIG. 4. Coherence of two unmeasured qubits coupled to a common when the target qubit is measured. (a) Sequence for a Ramsey experiment with fixed length. Between two qubit rotations of $\pi/2$ (where ϕ indicates around what axis) either the measurement pulse (red) is applied or not. To mimic a decoupled quantum computation, N echo pulses are inserted between the two $\pi/2$ pulses. (b) Ramsey fringes while performing one echo pulse. The triangles and solid lines are respectively the data and fit for the control experiment. The circles and dashed lines are the data and fit when the target qubit is measured. The two curves are phase-shifted due to the Stark-shift. The y-axis is normalized to the contrast of the control experiment. The experiment is performed on two different qubits (yellow and green) and the data are shown with opposite phases for clarity. In (c) we show the evolution of the coherence for different numbers of echo pulses. The Ramsey contrasts are normalized by the amplitude of their respective control experiment.

surement results are highly correlated with the previous one. Some rare measurement results display discrete transitions from one state to another. To estimate the fidelity, we plot in Fig. 3(b) the measurement distribution after a first stringent post-selection measurement: if the first measurement yields a value $I < \bar{I}_{|g\rangle}$ (resp. $I > \bar{I}_{|e\rangle}$), where the bar indicates the average of the distribution, we count the second measurement as being post-selected on $|g\rangle$ (resp. $|e\rangle$). This selection does not eliminate the spurious thermal population in the excited $|f\rangle$ state. We fit each distribution with a Gaussian and adjust a threshold to minimize the readout errors. We define the fidelities for the state $|g\rangle$ ($|e\rangle$) as $\mathcal{F}_g = 1 - p(g|e)$ ($\mathcal{F}_e = 1 - p(e|g)$), where $p(i|j)$ is the probability to measure the state i if the qubit was initialized in j. We find $\mathcal{F}_g = 99.3\%$ and $\mathcal{F}_e = 98.5\%$. From this, we define the total fidelity $\mathcal{F} = 1 - p(e|g) - p(g|e) = 97.8\%$. On the other hand, the QND-ness is defined as $\mathcal{Q} = (p_{e,e} + p_{g,g})/2$, where $p_{i,i}$ is the probability to measure the state i twice in two successive measurements. We find $\mathcal{Q} = 98.4\%$. In practice $\mathcal{F}$ and $\mathcal{Q}$ are mainly limited by the energy relaxation of the qubit.

Finally, we present how selective our measurement is in a multi-qubit architecture, which comprises 3 qubits coupled to the same readout resonator. The two qubits that are not targeted by the measurement have a dispersive coupling to the readout resonator that is similar to the dispersive coupling of the main qubit χ ($\ll \kappa$) and a T_2 of 30 μs. As a consequence, when the target qubit is measured, the unmeasured qubits are dephased by the photon shot noise of the coherent state with a number of photons $\bar{n}_{tot} = |\alpha_m|^2/4$. With $\chi \ll \kappa$, the dephasing rate is at worst of order $\bar{n}_{tot}(\chi/\kappa)^2\kappa$ and should be much smaller than the measurement rate of the target qubit [22]. However, this dephasing is not inevitable since it can be mitigated by applying a dynamical decoupling sequence of pulses to the unmeasured qubits [15, 33]. In fact, any realistic quantum computation on the unmeasured qubits would use such a dynamical decoupling sequence of pulses to mitigate environmental dephasing, which is often the main source of decoherence in cQED. Hence, the spurious dephasing due to the selective measurement will also be suppressed without having to adapt the pulse sequence on the unmeasured qubits. While measuring the target qubit, we assess the decoherence of the unmeasured qubits with a fixed-length Ramsey sequence with N interleaved π-pulses on the unmeasured qubits (Fig. 4(a)). As shown in Fig. 4(b), the Ramsey contrast for both unmeasured qubits is nearly independent of whether the target qubit is measured or not. In Fig. 4(c) we plot the ratio between the amplitudes in these two cases and observe that the measurement pulse adds at most 10% of

dephasing with no decoupling. Moreover, it is completely eliminated by inserting a few echo pulses in the Ramsey sequence.

In conclusion, we have realized a new readout method for the state of superconducting qubits, in which the information of the qubit is coupled to a displacement along a single quadrature of a readout resonator. We have demonstrated fast and selective QND readout with this coupling in a multi-qubit architecture. This coupling is strong even when the dispersive shift is more than an order of magnitude smaller than the linewidth of the resonator, which can be beneficial to the coherence of the qubits. Our readout scheme can be made even faster with further optimizations of the system. More importantly, unlike the dispersive readout, our displacement readout can provide exponentially improved sensitivity by squeezing the microwave photons incident on the readout resonator [12, 14]. The interaction we engineered is also useful beyond the readout of superconducting qubits. It can be applied to multi-qubit gates [10, 11, 34, 35], to the creation and correction of GKP codes [36] and pair-cat codes [37], and to single-photon [38] and photon-parity [39] detection.

We acknowledge U. Vool and P. Campagne-Ibarcq for helpful discussions. Facilities use was supported by the Yale SEAS clean room and the Yale Institute for Nanoscience and Quantum Engineering (YINQE). This research was supported by the Army Research Office (ARO) under Grants No. W911NF-14-1-0011, W911NF-18-1-0212 and W911NF-14-1-0563.

* steven.touzard@yale.edu
† michel.devoret@yale.edu

[1] D. P. DiVincenzo, Fortschritte der Physik **48**, 771 (2000).
[2] S. Haroche and J. Raimond, *Exploring the Quantum: Atoms, Cavities and Photons.* (Oxford University Press, 2006).
[3] A. Blais, R.-S. Huang, A. Wallraff, S. M. Girvin, and R. J. Schoelkopf, Phys. Rev. A **69**, 062320 (2004).
[4] A. Wallraff, D. I. Schuster, A. Blais, L. Frunzio, R. S. Huang, J. Majer, S. Kumar, S. M. Girvin, and R. J. Schoelkopf, Nature **431**, 162 (2004).
[5] J. Gambetta, A. Blais, M. Boissonneault, A. A. Houck, D. I. Schuster, and S. M. Girvin, Phys. Rev. A **77**, 1 (2008).
[6] T. Picot, A. Lupacscu, S. Saito, C. J. P. M. Harmans, and J. E. Mooij, Phys. Rev. B **78**, 132508 (2008).
[7] M. Boissonneault, J. M. Gambetta, and A. Blais, Phys. Rev. A **79**, 013819 (2009).
[8] D. H. Slichter, R. Vijay, S. J. Weber, S. Boutin, M. Boissonneault, J. M. Gambetta, A. Blais, and I. Siddiqi, Phys. Rev. Lett. **109**, 153601 (2012).
[9] D. Sank, Z. Chen, M. Khezri, J. Kelly, R. Barends, B. Campbell, Y. Chen, B. Chiaro, A. Dunsworth, A. Fowler, E. Jeffrey, E. Lucero, A. Megrant, J. Mutus, M. Neeley, C. Neill, P. J. J. O'Malley, C. Quintana, P. Roushan, A. Vainsencher, T. White, J. Wenner, A. N. Korotkov, and J. M. Martinis, Phys. Rev. Lett. **117**, 190503 (2016).
[10] A. J. Kerman, New J. Phys. **15**, 123011 (2013).
[11] P. M. Billangeon, J. S. Tsai, and Y. Nakamura, Phys. Rev. B **91**, 094517 (2015).
[12] N. Didier, J. Bourassa, and A. Blais, Phys. Rev. Lett. **115**, 203601 (2015).
[13] M. Aspelmeyer, T. J. Kippenberg, and F. Marquardt, Rev. Mod. Phys. **86**, 1391 (2014).
[14] A. Eddins, S. Schreppler, D. M. Toyli, L. S. Martin, S. Hacohen-Gourgy, L. C. G. Govia, H. Ribeiro, A. A. Clerk, and I. Siddiqi, Phys. Rev. Lett. **120**, 040505 (2018).
[15] L. Viola, S. Lloyd, and E. Knill, Phys. Rev. Lett. **83**, 4888 (1999).
[16] A. A. Clerk, M. H. Devoret, S. M. Girvin, F. Marquardt, and R. J. Schoelkopf, Rev. Mod. Phys. **82**, 1155 (2010).
[17] J. Suh, A. J. Weinstein, C. U. Lei, E. E. Wollman, S. K. Steinke, P. Meystre, A. A. Clerk, and K. C. Schwab, Science **344**, 1262 (2014).
[18] D. Vion, A. Aassime, A. Cottet, P. Joyez, H. Pothier, C. Urbina, D. Esteve, and M. H. Devoret, Science **296**, 886 (2002).
[19] T. Roy, S. Kundu, M. Chand, S. Hazra, N. Nehra, R. Cosmic, A. Ranadive, M. P. Patankar, K. Damle, and R. Vijay, Phys. Rev. Applied **7**, 054025 (2017).
[20] C. Eichler and J. R. Petta, Phys. Rev. Lett. **120**, 227702 (2018).
[21] Z. Leghtas, S. Touzard, I. M. Pop, A. Kou, B. Vlastakis, A. Petrenko, K. M. Sliwa, A. Narla, S. Shankar, M. J. Hatridge, M. Reagor, L. Frunzio, R. J. Schoelkopf, M. Mirrahimi, and M. H. Devoret, Science **347**, 853 (2015).
[22] See Supplemental Material for details, which includes Ref. [40].
[23] D. I. Schuster, A. A. Houck, J. A. Schreier, A. Wallraff, J. M. Gambetta, A. Blais, L. Frunzio, J. Majer, B. Johnson, M. H. Devoret, S. M. Girvin, and R. J. Schoelkopf, Nature **445**, 515 (2007).
[24] A. A. Houck, J. A. Schreier, B. R. Johnson, J. M. Chow, J. Koch, J. M. Gambetta, D. I. Schuster, L. Frunzio, M. H. Devoret, S. M. Girvin, and R. J. Schoelkopf, Phys. Rev. Lett. **101**, 080502 (2008).
[25] J. Gambetta, A. Blais, D. I. Schuster, A. Wallraff, L. Frunzio, J. Majer, M. H. Devoret, S. M. Girvin, and R. J. Schoelkopf, Phys. Rev. A **74**, 042318 (2006).
[26] A. P. Sears, A. Petrenko, G. Catelani, L. Sun, H. Paik, G. Kirchmair, L. Frunzio, L. I. Glazman, S. M. Girvin, and R. J. Schoelkopf, Phys. Rev. B **86**, 1 (2012).
[27] M. Reagor, W. Pfaff, C. Axline, R. W. Heeres, N. Ofek, K. Sliwa, E. Holland, C. Wang, J. Blumoff, K. Chou, M. J. Hatridge, L. Frunzio, M. H. Devoret, L. Jiang, and R. J. Schoelkopf, Phys. Rev. B **94**, 014506 (2016).
[28] N. E. Frattini, V. V. Sivak, A. Lingenfelter, S. Shankar, and M. H. Devoret, Phys. Rev. Applied **10**, 054020 (2018).
[29] J. Gambetta, W. A. Braff, A. Wallraff, S. M. Girvin, and R. J. Schoelkopf, Phys. Rev. A **76**, 012325 (2007).
[30] C. A. Ryan, B. R. Johnson, J. M. Gambetta, J. M. Chow, M. P. da Silva, O. E. Dial, and T. A. Ohki, Phys. Rev. A **91**, 022118 (2015).
[31] C. C. Bultink, B. Tarasinski, N. Haandbæk, S. Poletto, N. Haider, D. J. Michalak, A. Bruno, and L. DiCarlo,

Appl. Phys. Lett. **112**, 092601 (2018).
[32] D. T. McClure, H. Paik, L. S. Bishop, M. Steffen, J. M. Chow, and J. M. Gambetta, Phys. Rev. Applied **5**, 011001 (2016).
[33] D. A. Lidar, Adv. Chem. Phys. **154**, 295 (2014).
[34] S. Richer and D. Divincenzo, Phys. Rev. B **93** (2016).
[35] B. Royer, A. L. Grimsmo, N. Didier, and A. Blais, Quantum **1**, 11 (2017).
[36] B. M. Terhal and D. Weigand, Phys. Rev. A **93**, 012315 (2016).
[37] V. V. Albert, S. O. Mundhada, A. Grimm, S. Touzard, M. H. Devoret, and L. Jiang, arXiv:1801.05897 (2018).
[38] B. Royer, A. L. Grimsmo, A. Choquette-Poitevin, and A. Blais, Phys. Rev. Lett. **120**, 203602 (2018).
[39] S. Puri, A. Grimm, P. Campagne-Ibarcq, A. Eickbusch, K. Noh, G. Roberts, L. Jiang, M. Mirrahimi, M. H. Devoret, and S. M. Girvin, arXiv:1807.09334 (2018).
[40] J. Z. Blumoff, K. Chou, C. Shen, M. Reagor, C. Axline, R. T. Brierley, M. P. Silveri, C. Wang, B. Vlastakis, S. E. Nigg, L. Frunzio, M. H. Devoret, L. Jiang, S. M. Girvin, and R. J. Schoelkopf, Phys. Rev. X **6**, 31041 (2016).